Supplementary Information (SI) for Journal of Materials Chemistry C.

Supplementary materials

Online and offline learning using fading memory functions in HfSiOx-based ferroelectric tunnel junction

Jungwoo Lee†[a], Chaewon Youn†[a], Jungang Heo[a], and Sungjun Kim*[a]

[a] Division of Electronics and Electrical Engineering, Dongguk University, Seoul 04620, South Korea

E-mail: sungjun@dongguk.edu

†The authors contributed equally to this work.

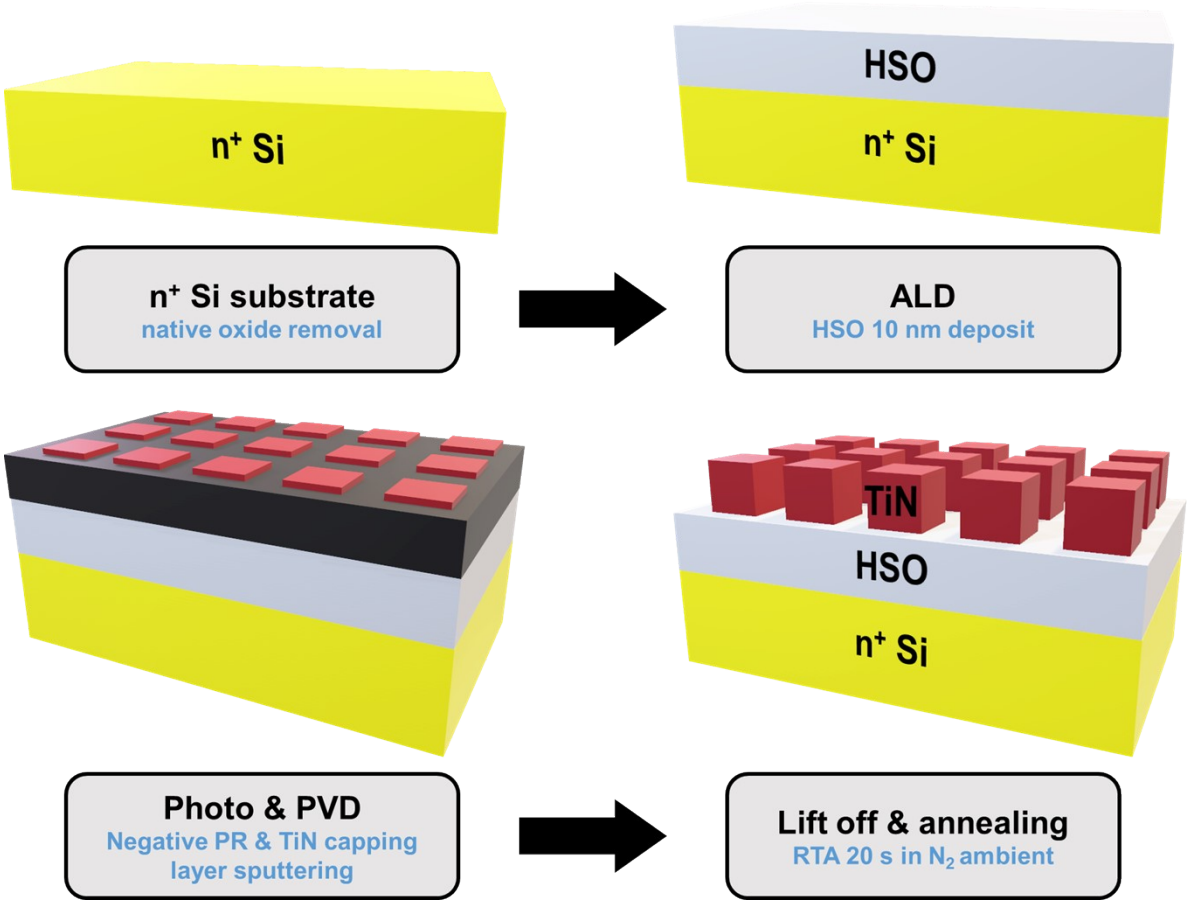

Fig. S1 TiN/HSO/n+Si device fabrication process flow.

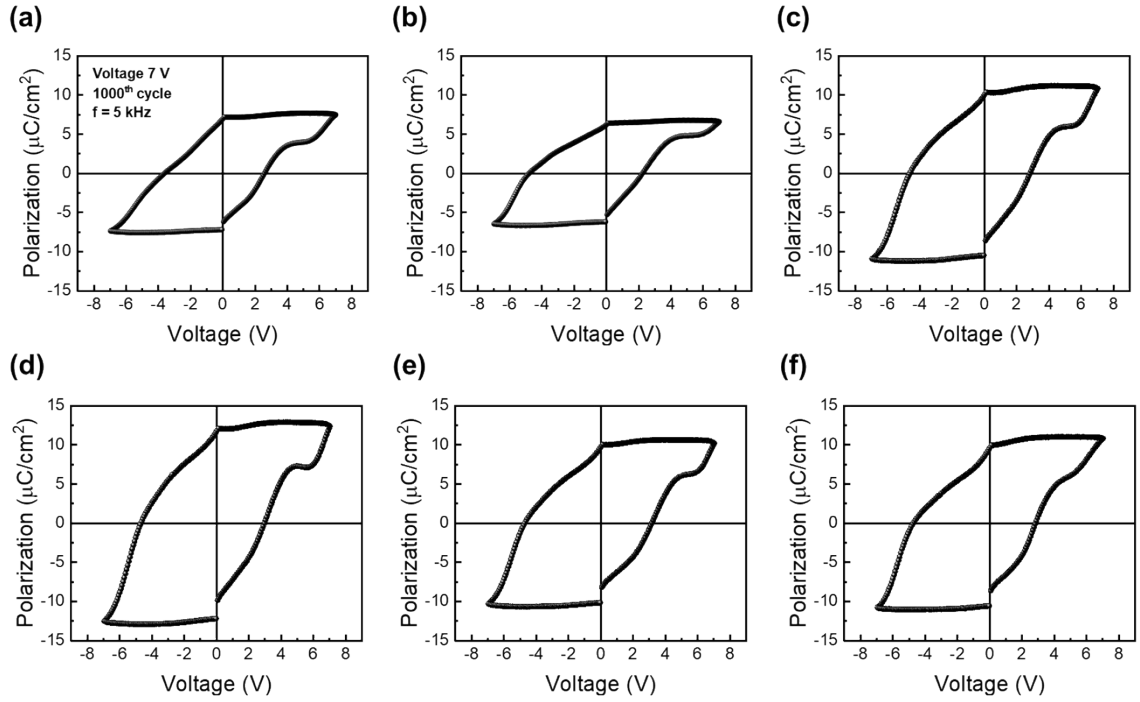

Fig. S2: Polarization-voltage curves annealed at (a) 600 °C, (b) 650 °C, (c) 700 °C, (d) 750 °C, (e) 800 °C, and (f) 850 °C.

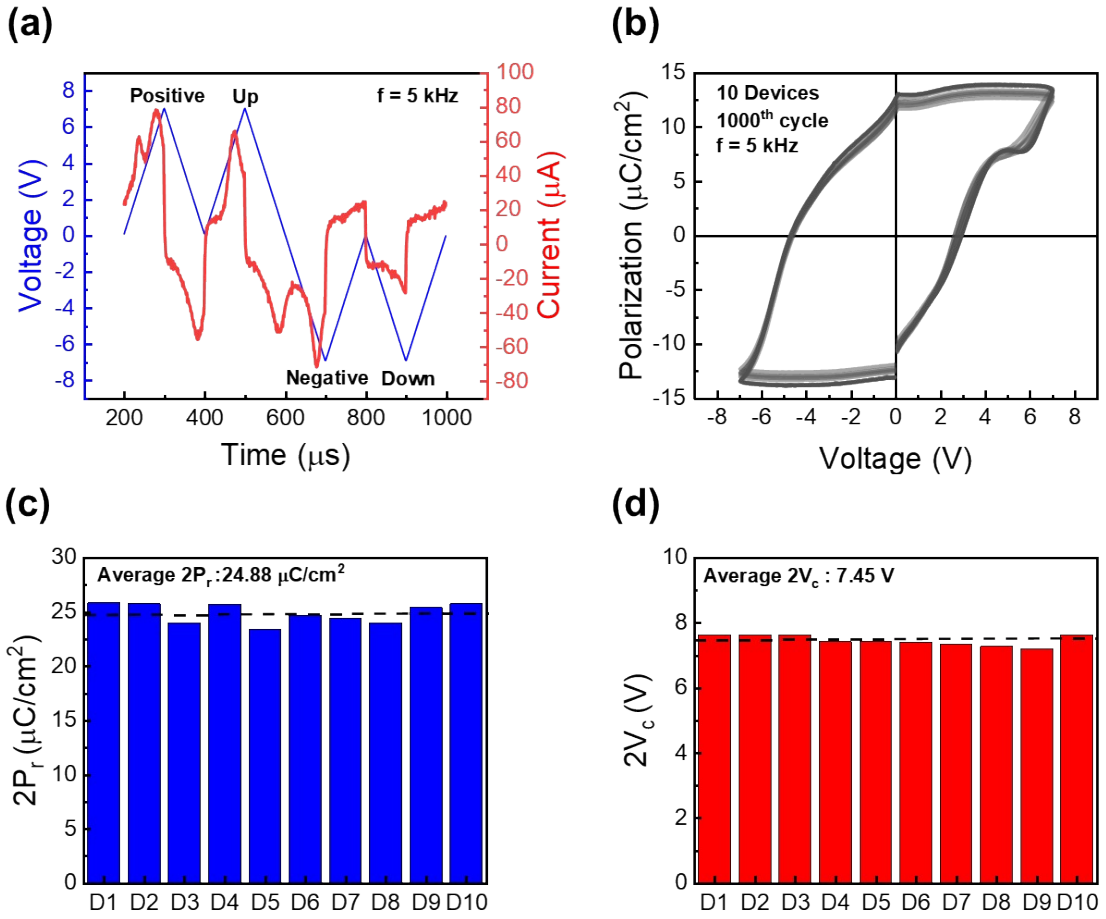

Fig. S3 (a) Pulse scheme of PUND and current response. (b) Polarization-voltage curve for 10 devices annealed at 750 °C. (c) Extracted $2P_r$ value for 10 devices. d) Extracted $2V_c$ value for 10 devices.

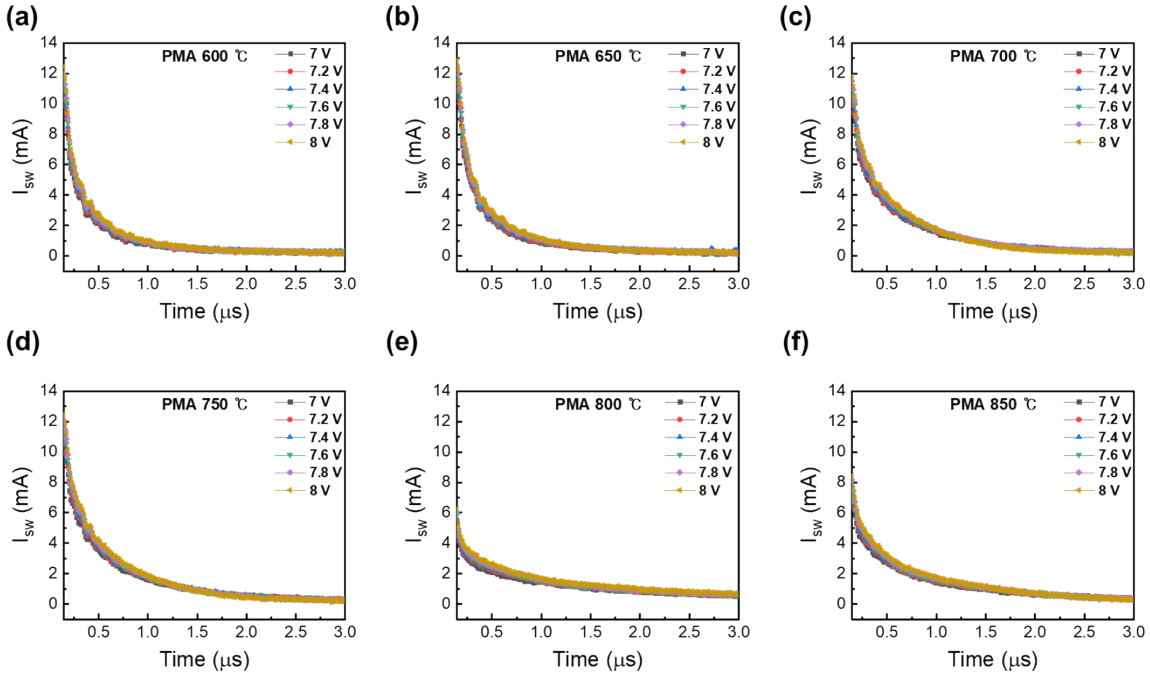

Fig. S4 Exponentially fitted curves after t_0 for devices annealed at (a) 600 °C, (b) 650 °C, (c) 700 °C, (d) 750 °C, (e) 800 °C, and (f) 850 °C.

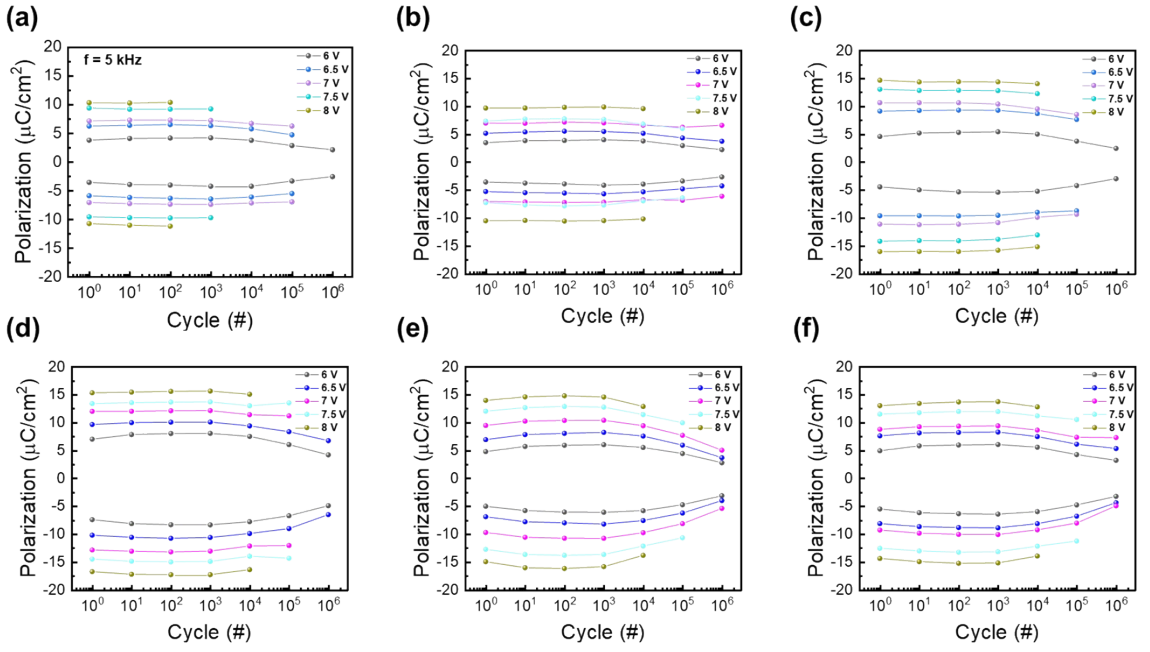

Fig. S5 Endurance characteristics for devices annealed at (a) 600 °C, (b) 650 °C, (c) 700 °C, (d) 750 °C, (e) 800 °C, and (f) 850 °C.

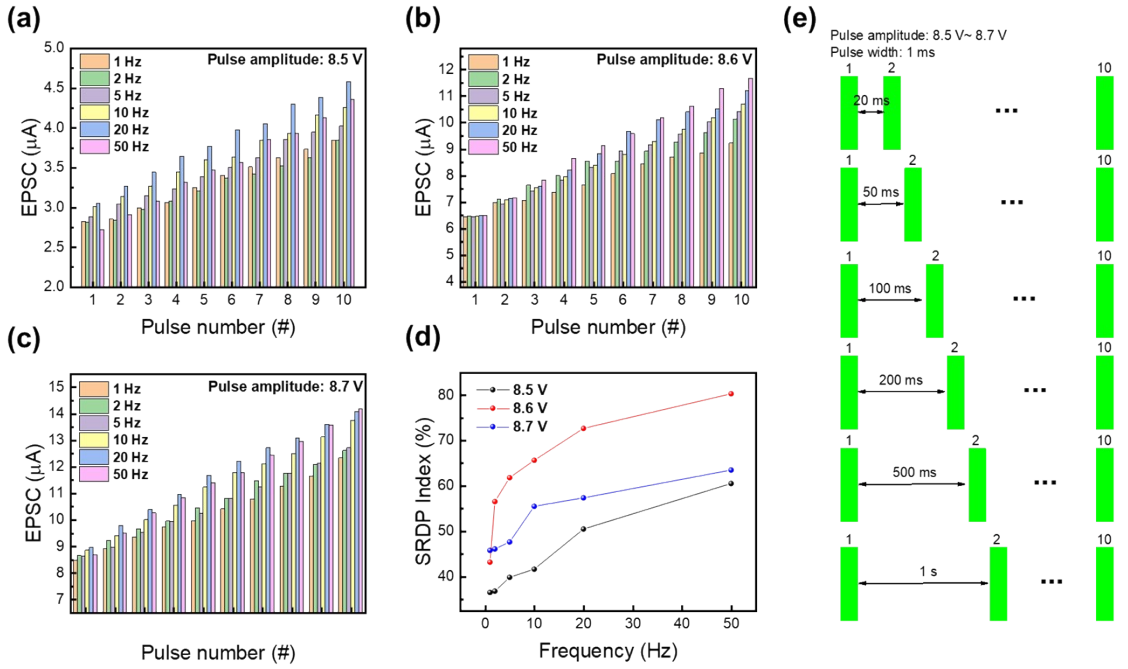

Fig. S6 EPSC response based on the different frequency ranges applied in 10 consecutive pulses at (a) 8.5 V, (b) 8.6 V, and (c) 8.7 V. (d) SRDP index for various voltage range (from 8.5 to 8.7 V). (e) Pulse scheme of SRDP.

Fig. S6(a)-(c) shows the results of the excitation postsynaptic current (EPSC) when the frequency is varied across different voltage ranges. These results align with the SRDP characteristics, where synaptic plasticity and neuronal firing change with increasing frequency. The pulse scheme used is illustrated in Figure S6e, where 10 identical pulses were applied at varying frequencies. In typical SRDP, a decrease in frequency corresponds to an increase in interval time, resulting in a postsynaptic current that gradually weakens. This is summarized in Fig. S6(d) as the SRDP index using the following equation.

$$SRDP\ index = \frac{(I_{10} - I_1)}{I_{10}} \times 100$$

As the frequency increases, higher SRDP index values are observed across all voltage ranges, indicating that our device effectively mimics SRDP behavior.

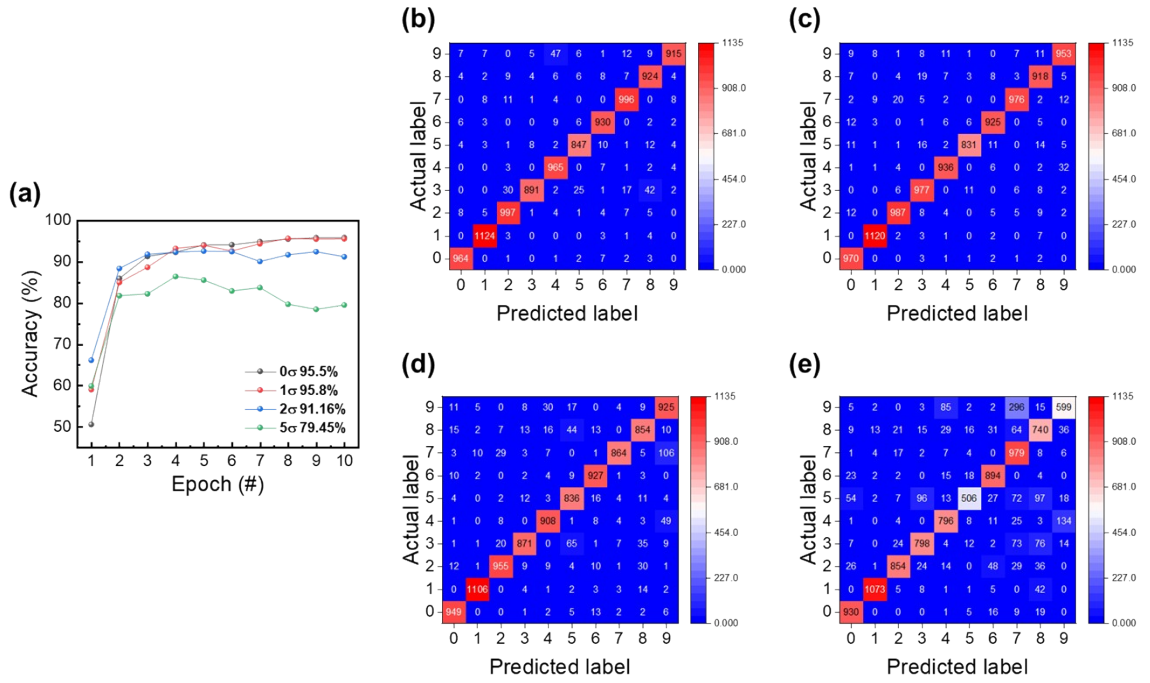

Fig. S7 (a) Pattern recognition accuracy as standard deviation values increase from 0σ to 5σ based on cycle-to-cycle variation; Confusion matrix after training for the model of (b) 0σ, (c) 1σ, (d) 2σ, and (e) 5σ.

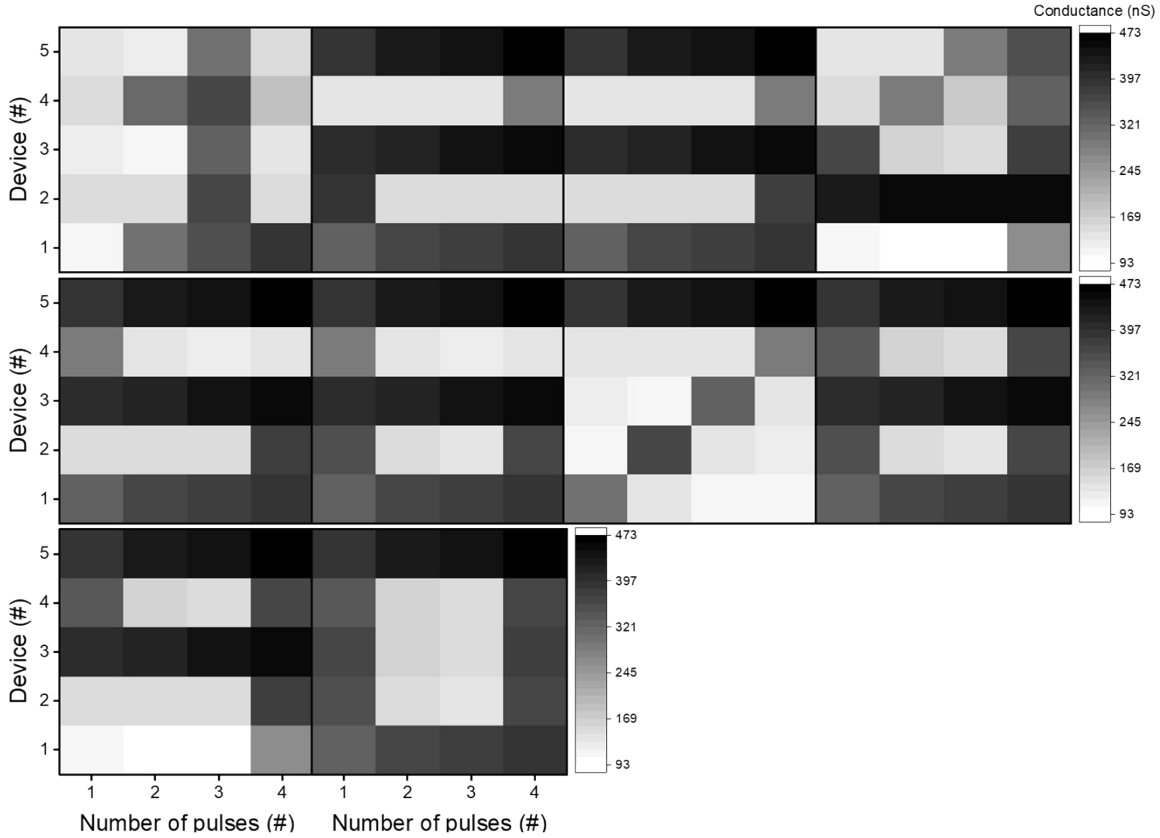

Fig. S8 Number images from 0 to 9, implemented through reservoir computing, combined from conductance data of five different devices.

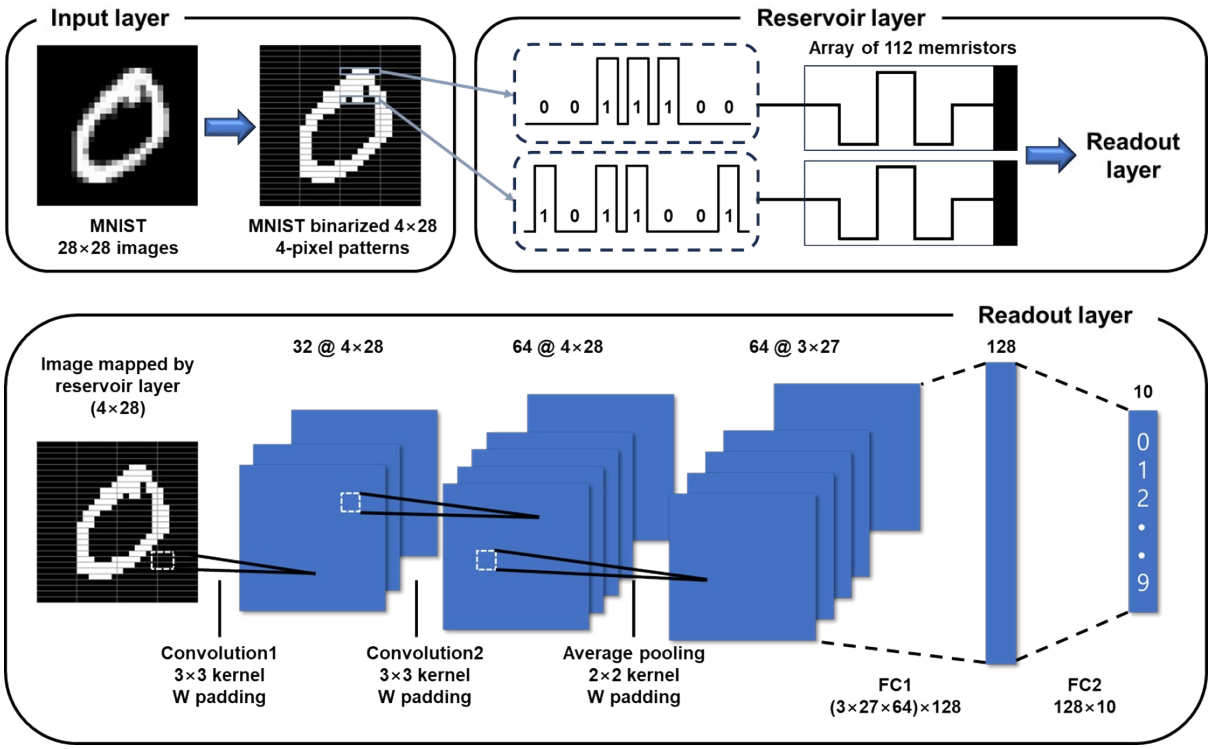

Fig. S9 Schematic illustration of the 7-bit reservoir computing system used for patter recognition in offline learning.

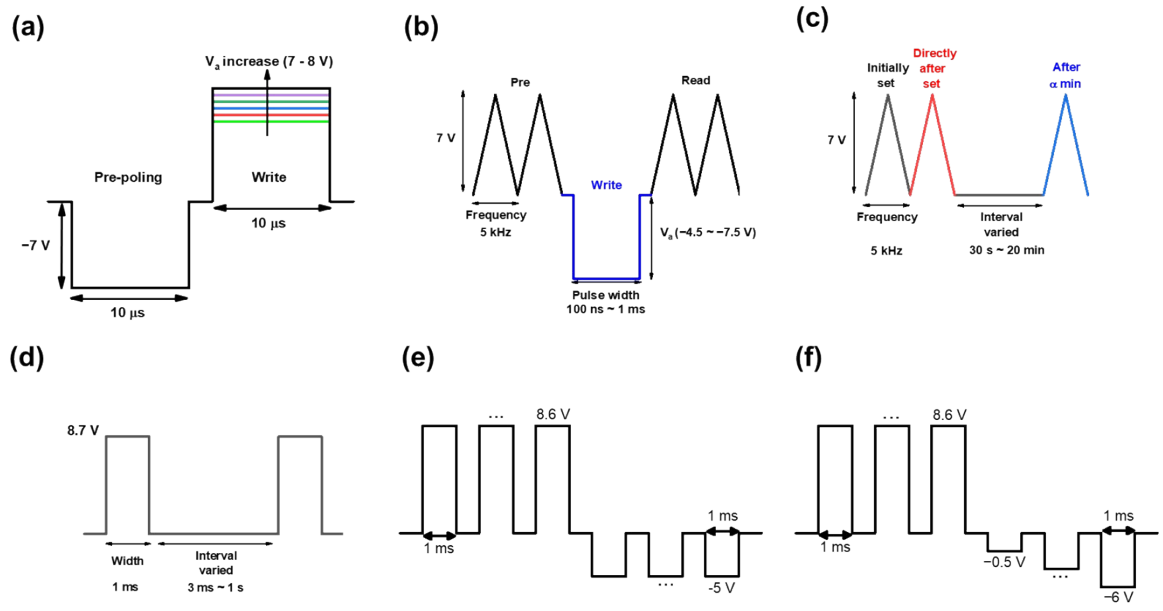

Fig. S10 Pulse scheme of (a) short pulse switching technique, and (b) switching speed. (c) Investigation of depolarization effect by varying pulse interval. (d) Pulse scheme of PPF. (e) Identical pulse scheme of potentiation and depression. (f) Incremental pulse scheme of potentiation and depression.

Table. S1 Comparison of the functions of the TiN/HSO/n^+Si ftj to previously reported studies.

Device Scheme	Memory Characteristic	Retention	Endurance	PPF	TER	Reservoir computing		Ref.
						Application implementation	Recognition accuracy	
TiN/HSO/SiON/n^+ Si	Long-term memory	-	10^4 ~ 10^5	No	-	No	-	S1
TiN/Al_2O_3/HSO/SiO_2/ n^+ Si	Long-term memory	10 years	10^5	No	-	No	-	S2
TiN/HSO/SiON/Si	Long-term memory	10^5 s	10^3	No	700	No	-	S3
TiN/HSO/SiN/Si	Long-term memory	10 years	10^4	No	-	No	-	S4
TiN/HSO/TiN/HfO_2/ SiO_2/Si	Long -term memory	-	10^5	No	-	No	-	S5
TiN/HSO/SiN/Si	Long-term memory	10 years	10^4	No	-	No		S6
TiN/HSO/n^+ Si	Short-term memory	-	10^6	Yes	~1099	Yes (7-bit)	97.5%	This work

Reference

S1 P. Duhan, T. Ali, P. Khedgarkar, K. Kühnel, M. Czernohorsky, M. Rudolph, R. Hoffmann, A. Sünbül, D. Lehninger, P. Schramm, T. Kämpfe and K. Seidel, *IEEE Transactions on Electron Devices*, 2023, **70**, 5645–5650.

S2 T. Ali, K. Mertens, R. Olivo, M. Rudolph, S. Oehler, K. Kühnel, D. Lehninger, F. Müller, R. Hoffmann, P. Schramm, K. Biedermann, J. Metzger, R. Binder, M. Czernohorsky, T. Kämpfe, J. Müller, K. Seidel, J. Van Houdt and L. M. Eng, *IEEE Transactions on Electron Devices*, 2021, **68**, 2098–2106.

S3 Y. Lee, S. Song, W. Ham and S.-E. Ahn, *Materials*, 2022, **15**, 2251.

S4 T. Ali, P. Polakowski, K. Kühnel, M. Czernohorsky, T. Kämpfe, M. Rudolph, B. Pätzold, D. Lehninger, F. Müller, R. Olivo, M. Lederer, R. Hoffmann, P. Steinke, K. Zimmermann, U. Mühle, K. Seidel and J. Müller, in *2019 IEEE International Electron Devices Meeting (IEDM)*, 2019, p. 28.7.1-28.7.4.

S5 T. Ali, K. Mertens, R. Olivo, D. Lehninger, M. Lederer, F. Müller, M. Rudolph, S. Oehler, K. Kühnel, R. Hoffmann, P. Schramm, M. Czernohorsky, T. Kämpfe and K. Seidel, in *2022 International Symposium on VLSI Technology, Systems and Applications (VLSI-TSA)*, 2022, pp. 1–2.

S6 T. Ali, K. Kühnel, R. Olivo, D. Lehninger, F. Müller, M. Lederer, M. Rudolph, S. Oehler, K. Mertens, R. Hoffmann, K. Zimmermann, P. Schramm, J. Metzger, R. Binder, M. Czernohorsky, T. Kämpfe, K. Seidel, J. Müller, J. Van Houdt and L. M. Eng, *Electronic Materials*, 2021, **2**, 344–369.